IEEE Access
Multidisciplinary | Rapid Review | Open Access Journal

Received April 19, 2019, accepted May 6, 2019, date of publication May 8, 2019, date of current version May 20, 2019.

Digital Object Identifier 10.1109/ACCESS.2019.2915628

Polarization-Reconfigurable Cylindrical Dielectric Resonator Antenna Excited by Dual Probe With Tunable Feed Network

BEI-JIA LIU[1], JING-HUI QIU[1], CHANG-HUI WANG[1], WEI LI[1], AND GUO-QIANG LI[2]

[1]Department of Microwave Engineering, Harbin Institute of Technology, Harbin 150001, China
[2]Department of Automatic Image Recognition, Harbin Kejia General Mechanical and Electrical Company, Harbin 150060, China

Corresponding author: Bei-Jia Liu (liubeijia@hit.edu.cn)

This work was supported in part by the National Natural Science Foundation of China under Grant No. U1633202 and Grant No. 61731007.

ABSTRACT A polarization-reconfigurable cylindrical dielectric resonator antenna (DRA) based on a tunable feed network is presented in this paper. $HEM_{11\delta}$ modes excited by two-port side-fed probes are adapted to design the proposed DRA. Polarization reconfigurable characteristic can be obtained by a tunable feed network that consists of Wilkinson equal power divider, parasitic elements used for phase shifters, and p-i-n diodes between them. By controlling the four pairs of p-i-n diode switches to active corresponding elements as effective phase shifters, two sources with equal amplitude and 0° or ±90° phase differences are obtained to generate linear-polarized (LP) or circular-polarized (CP) states, respectively. A fully functional prototype of the proposed antenna with the dimension of $0.55\lambda \times 0.55\lambda \times 0.14\lambda$ has been designed, fabricated, and tested. The results indicate that the proposed DRA can achieve the bandwidths of more than 30% for both impedance bandwidth and 3-dB axial ratio bandwidth at CP states, and two LP states with the impedances of 6.3% and 9.5%. Stable directional patterns and realized gains are obtained for all the states. These performances make the proposed DRA suitable for polarization diversity scenarios in communication systems.

INDEX TERMS Cylindrical dielectric resonator antenna, $HEM_{11\delta}$ mode, polarization reconfiguration, Wilkinson power divider, p-i-n diodes.

I. INTRODUCTION

Dielectric resonator antenna (DRA) has been a research hotspot over the past three decades for its extraordinary features of compact size, light weight, high efficiency, flexible design freedom and easy to excite. There are a lot of publications to report the achievements of how to excite different modes, broaden bandwidth, generate circular polarization (CP), obtain dual polarization, achieve reconfiguration and apply in high frequency for DRA [1]–[10].

At the same time, reconfigurable antennas, which can change operation frequency, radiation pattern and polarization mode to accommodate the system requirement, have been extensively studied since 1983 [11]–[15]. Polarization reconfigurable antennas has attracted attention and been put into research for different applications. At present, a lot of polarization reconfigurable antennas have been proposed for slot antennas or patch antennas to switch among linear polarization (LP), right-handed circular polarization (RHCP) and left-handed polarization (LHCP). One common insufficiency is the narrow operation bandwidth, especially for axial ratio bandwidth of CP state [16]–[22]. To overcome the problem, some mechanisms are researched and published, including polarization-rotation artificial magnetic conductor, cross-probe, magneto-electric dipole and so on [23]–[28]. In addition, DRA is a promising candidate for achieving polarization reconfigurable design and there have been few research achievements to certificate the feasibility. Electronically reconfigurable DRA with multiple polarization states is proposed based on rectangular dielectric resonator (DR) in [29], whose impedance bandwidths at all states are above 20% and axial ratio bandwidth is only 1% or so. In [30], the similar cross slot is adopted, and a lattice structure is put into the DR, which improves the axial ratio bandwidth and obtains a broadband CP states with 3-dB axial ratio bandwidth of 20.7%. A novel liquid DRA with agile CP states is

The associate editor coordinating the review of this manuscript and approving it for publication was Kwok L. Chung.

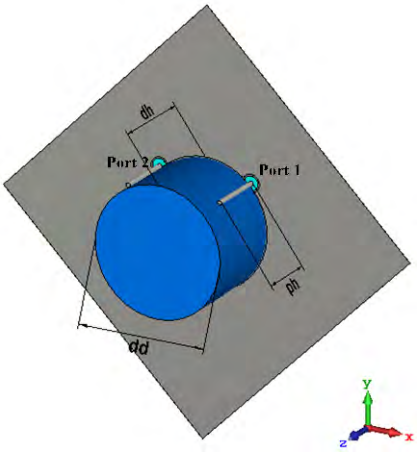

FIGURE 1. Configuration of the adjacently probe-fed cylindrical DRA.

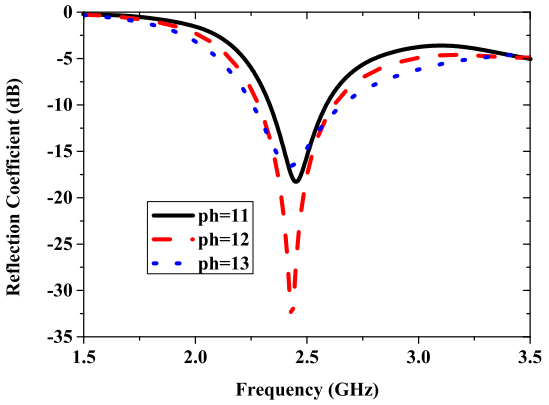

FIGURE 2. Effects of probe length on reflection coefficients with Port 1 feed.

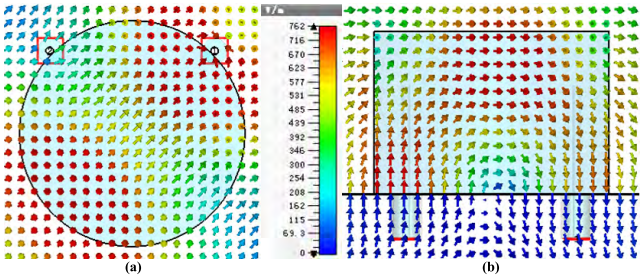

FIGURE 3. Field distributions of $HEM_{11\delta}$ mode of the DRA with Port 1 feed at: (a) xoy-plane and (b) yoz-plane.

investigated in [31], which needs 3-D printing container and extra pump to make the antenna transform between RHCP state and LHCP state with common axial ratio bandwidth of 16.3%. However, to our best knowledge, there is no polarization reconfigurable DRA at CP state with impedance and axial ratio bandwidth both above 30%.

In this paper, we propose a polarization reconfigurable cylindrical DRA with tunable feed network. The cylindrical DR excited by probes at two ports is used for the design the antenna based on $HEM_{11\delta}$ mode. The tunable feed network consists of Wilkinson power divider, two pairs of shifters and four pairs of p-i-n diodes. It is used for providing two way signals of equal amplitude and equal phase or quadrature phase for cylindrical DR to achieve LHCP state, RHCP state or LP states. The following section provides the proposed DRA design composed by dual-port cylindrical DRA, tunable feed network and polarization reconfigurable DRA. Section III presents the results for different polarization state, and performance analysis. Brief summary and concise conclusion are drawn in Section IV.

II. ANTENNA DESIGN

The proposed antenna design integrates the cylindrical DRA based on $HEM_{11\delta}$ mode excited by dual-port probes with tunable feed network composed by two way power divider and shifters for achieving polarization reconfiguration with stable broadside radiation patterns, which is numerically modeled and optimized by an electromagnetic computation software CST microwave studio 2017.

A. DUAL-PORT CYLINDRICAL DRA PERFORMANCE

Fig.1 depicts the configuration of the adjacently probe-fed cylindrical DRA with excited $HEM_{11\delta}$ mode. It is designed at 2.45 GHz with a dielectric constant of 9.9, a diameter of $dd = 26$ mm and a height of $dh = 18$ mm, according to formula (1) (2) [2]. In addition, the probe-fed DRA can be matched by adjusting the length ph of the probe. When the cylindrical DR is excited by Port 1, the effects of probe length on reflection coefficient are demonstrated in Fig. 2. It is found that the resonant frequencies shift slightly around 2.45 GHz, and the maximum resonant intensity occurs at $ph = 12$ mm. For clarifying the operation mode of the adjacently probe-fed DRA further, electric field distributions at azimuthal xoy-plane and elevation yoz-plane are depicted in Fig. 3.

$$f = \frac{6.324c}{2\pi r\sqrt{\varepsilon_r + 2}}\left[0.27 + \frac{0.36}{2t} + 0.02(\frac{1}{2t})^2\right], \quad 0.17 \le t \le 2.5 \tag{1}$$

$$t = 2dh/dd \tag{2}$$

Fig. 4 shows the reflection coefficients with two-port feed DRA under equal amplitude and 0° or 90° phase difference. It is observed that the DRA with two-port feed has better resonant performance but shift to the high frequency a little when it is excited by 90° phase difference. Axial ratios of the dual probe-fed DRA with equal amplitude and 90° phase difference are shown in Fig. 5, which demonstrate a wide 3 dB axial ratio bandwidth covering the impedance bandwidth. The cylindrical DRA has the ability to generate LP and CP through switching phase difference between two ports for probes illustrated above. In addition, simulated far-field radiation patterns of the DRA of LP states and CP states at 2.45 GHz are presented in Fig. 6, which are both of good and consistent directional radiation characteristic with maximum gain above 6 dB.

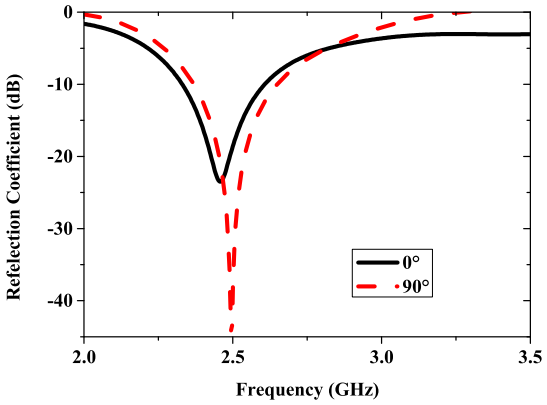

FIGURE 4. Reflection coefficients with two-port feed under equal amplitude and different phases.

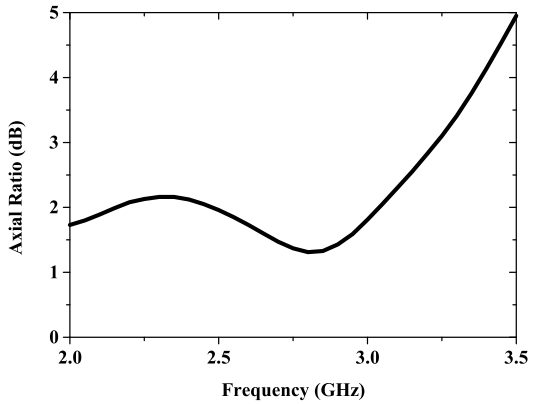

FIGURE 5. Axial ratios of the dual probe-fed DRA with equal amplitude and 90° phase difference.

B. TUNABLE FEED NETWORK

Fig. 7 shows the geometry of tunable feed network composed by microstrip feedline, Wilkinson equal power distributor and optional parasitic elements as phase shifters by p-i-n diodes, which are etched on the one side of the substrate with a dielectric constant of 3 and a height of 0.508 mm. The microstrip feedline has a width of $wm = 1.3$ mm corresponding to the characteristic impedance of $Z_0 = 50\Omega$. The two arms of Wilkinson power divider are quarter wavelength convertors with the width of $wc = 0.7$ mm corresponding to the characteristic impedance of $\sqrt{2}Z_0$. The output ports of the divider are connected a chip resistor with the value of $2Z_0$ and have a space of $\sqrt{2}dd$ for feeding the cylindrical DR mentioned in last section. The phase shifters symmetrically distributed are divided into two pairs: one for short pass-through shifters, and the other for long 90° phase shifters compared to the former. The two signals at port 2 and port 3 can have a phase difference of 90°, −90°, and 0°, depending on the states of eight p-i-n diodes. These diodes are denoted as ranging from D1 to D8, and two diodes control one shifter to decide whether the signal from divider go through the corresponding shifter or not. By tuning on the diodes of the two equal-length shifters, two signals at Port 2 and Port 3 are generated for LP. By tuning on the diodes of the

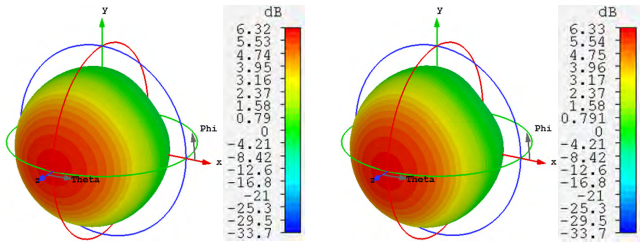

FIGURE 6. Simulated three-dimensional far-field radiation patterns for the DRA of LP states and CP states at 2.45 GHz: (a) equal amplitude and equal phase and (b) equal amplitude and 90° phase difference.

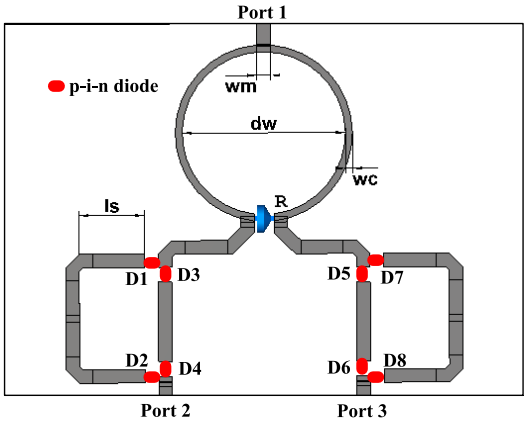

FIGURE 7. Geometry of tunable feed network.

two unequal-length shifters, two signals are generated for CP.

When the feed network is used for achieving LHCP or RHCP performance, one short shifter and one long shifter distributed on both sides are actuated by biasing circuit with four diodes ON, and the corresponding performances are as follows. Fig. 8 shows the input reflection coefficients of the tunable feed network for CP state with different *wc*, which indicates the resonant frequency shifts to the low frequency with the increase of divider radius *dw* and all have a wide impedance bandwidth, so $dw = 19$ is chosen for its good resonant intensity. Amplitude differences and phase differences of the transmission coefficients of between Port 1,2 and Port 1,3 with different ls for CP state are demonstrated in Fig. 9 and Fig. 10, and $ls = 6$ mm is chosen in this paper eventually.

C. POLARIZATION-RECONFIGURABLE DRA

Fig. 11 demonstrates the geometrical structure of the proposed polarization-reconfigurable cylindrical DRA with top view and back view, combining the dual-port DRA and tunable feed network as above. The square ground plane and substrate have a dimension of $sd = 75$ mm with a symmetrical corner cut of $sc = 18.3$ mm for soldering SMA firmly. One case of D3&&D4&&D7&&D8 ON and other diodes OFF is demonstrated by ideal breakover with metal bridge in Fig. 11(b), leading to CP for proposed DRA.

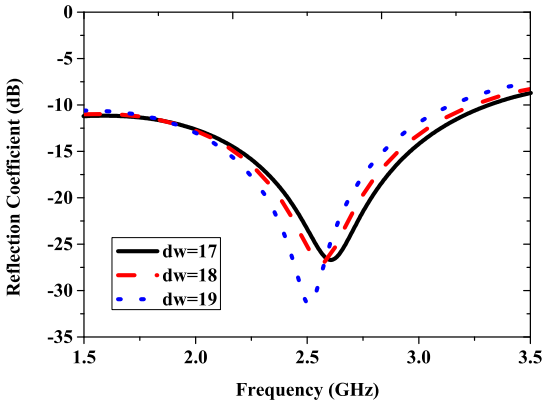

FIGURE 8. Reflection coefficients of the tunable feed network for CP state with different dw.

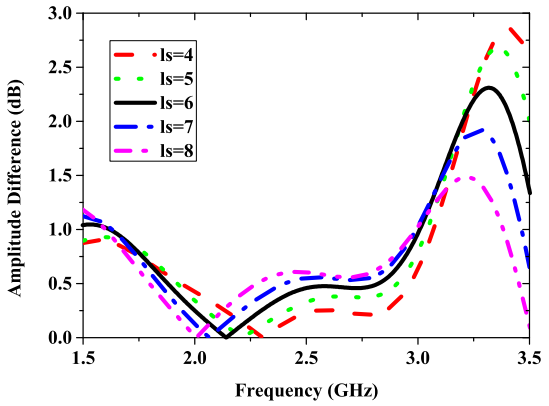

FIGURE 9. Amplitude differences of the transmission coefficients of between Port 1,2 and Port 1,3 for CP state.

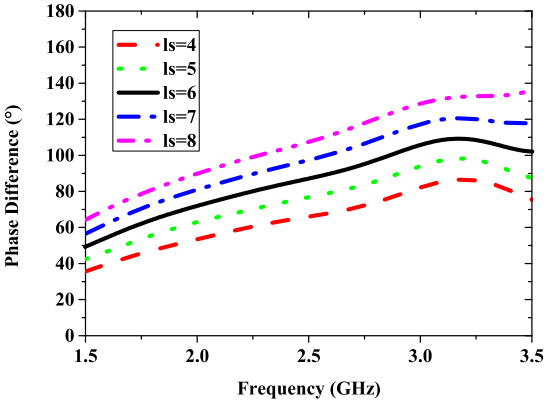

FIGURE 10. Phase differences of the transmission coefficients of between Port 1,2 and Port 1,3 for CP state.

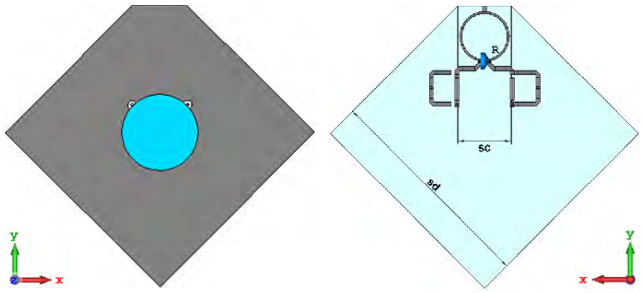

FIGURE 11. Configuration of the proposed polarization-reconfigurable cylindrical DRA: (a) top view and (b) back view.

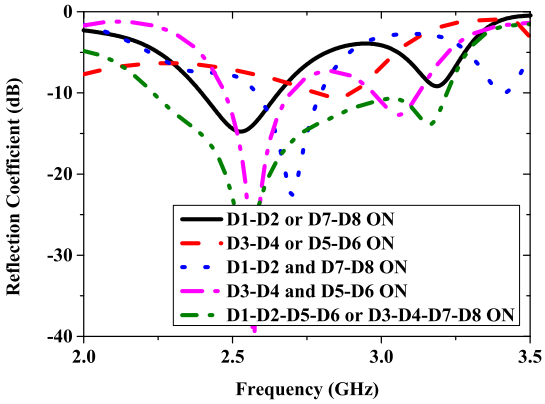

FIGURE 12. Reflection coefficients of the proposed DRA at different reconfigurable states.

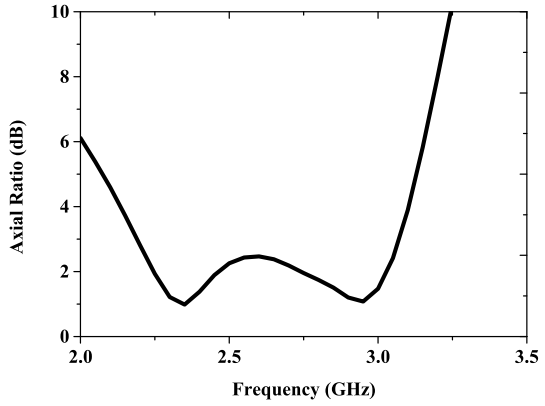

FIGURE 13. Axial ratios of the proposed DRA at CP states.

The input reflection coefficients of the proposed DRA at different reconfigurable states are depicted in Fig. 12. It can be observed that the states with only one activated shifter have poor impedance matching performance and are not considered effective state later. Two equal short shifters and two equal long shifters for the proposed DRA are both obtained better narrow bandwidths with different resonant frequencies. For the symmetry structure between two unequal shifters, identical impedance and axial ratio characteristics are obtained. It can be illustrated that the impedance characteristics occurs changes of varying degrees for the advent of Wilkinson power divider and different combinations of phase shifters and parasitic elements. For achieving CP, the unsymmetrical active phase shifters contribute to excite an effect higher mode and broad the impedance bandwidth based on the fusion of dominant mode and higher mode.

Fig. 13 shows the axial ratios for the proposed DRA reconfigured at CP states with 3 dB axial ratio bandwidth ranging from 2.18 GHz to 3.07 GHz. To verify the principle

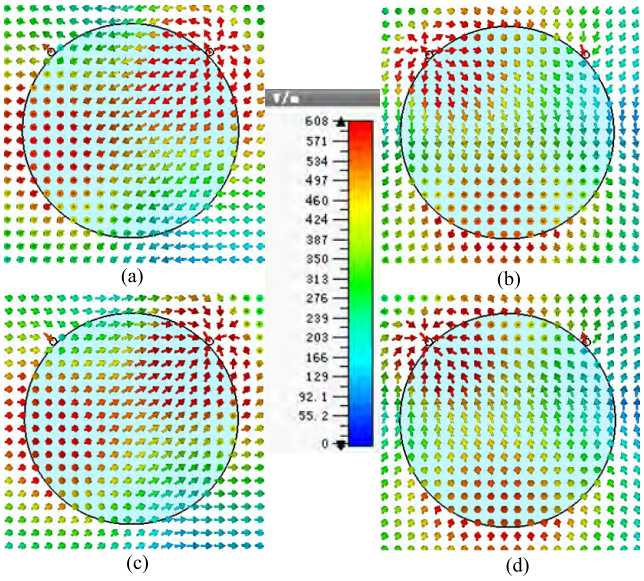

FIGURE 14. Simulated electric fields of the proposed DRA at RHCP state: (a) phase = 0 deg, (b) phase = 90 deg, (c) phase = 180 deg and (d) 270 deg.

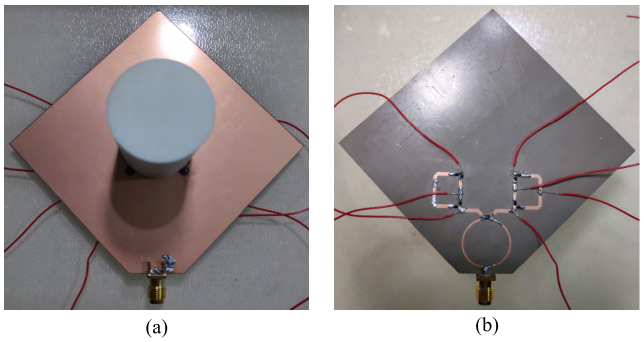

FIGURE 15. Prototype of the proposed polarization-reconfigurable cylindrical DRAs: (a) top view and (b) back view.

of the CP DRA, the simulated electric fields with different phases for the proposed cylindrical DRA are demonstrated in Fig. 14.With reference to the figure, the electric field vector rotates anticlockwise as the phase increases, which confirms the generation of RHCP.

III. RESULTS AND ANALYSIS

To validate the design, a prototype of polarization reconfigurable DRA operated at WLAN frequency bands was fabricated and tested. Fig. 15 shows the top view and back view for the prototype with effective states listed in Table 1. The cylindrical DR is made of aluminous ceramic and the p-i-n diodes (BAR 64-02 V) from Infineon are adopted as switches. The diode is modeled as a low forward resistance of 2.1 Ω for the ON-state with a forward voltage of 0.7 V and a high reverse resistance of 3 kΩ and a capacitor of 0.15 pF in parallel for the OFF-state. In the measurement, it is found that there is no need to introduce RF choke inductor between diodes and dc-lines, because the signal from instrument is too

TABLE 1. Effective switches state of the proposed feed network.

State	D1&&D2	D3&&D4	D5&&D6	D7&&D8	Polarization
I	ON	OFF	ON	ON	LHCP
II	OFF	ON	OFF	ON	RHCP
III	OFF	ON	ON	OFF	LP-1
IV	ON	OFF	OFF	ON	LP-2

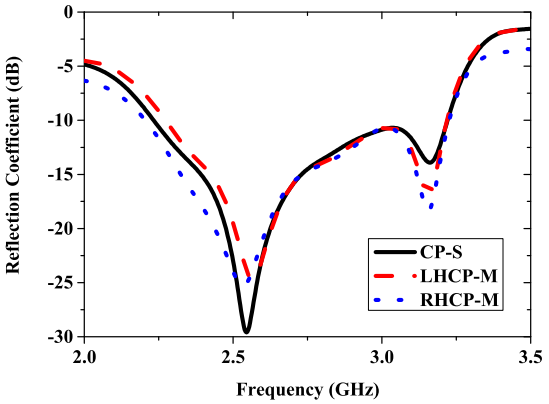

FIGURE 16. Simulated and measured input reflection coefficients when the proposed DRA is configured at CP states.

slim to influence the dc power. And a dc-block SMA connector is needed to protect vector network analyzer between the proposed DRA and measurement cable. The simplified bias circuit benefits avoiding distractions to antenna performance. When tested, some methods by making the cables at symmetrical positions and perpendicular to the adjacent metal strip are adopted to eliminate this cable effect as much as possible. The impedance bandwidth tests are performed by Agilent-N5227A network analyzer, and the far-field radiation characteristics are tested in the microwave anechoic chamber with the space dimension of 10m×6m×6m.

A. CIRCULAR-POLARIZED STATES

Fig. 16 shows the simulated and measured input reflection coefficients of the proposed DRA operated at CP states. The simulated reflection coefficients of LHCP and RHCP with impedance bandwidth of 34.3% (2.27-3.21 GHz) and 36.6% (2.23-3.23 GHz) are not exactly identical as simulations with impedance bandwidth of 36.3% (2.23-3.22 GHz). The measured impedance bandwidths are a little larger or smaller than the simulated one because of the influences in the dc biasing network, the inevitable errors in the process fabrication, integration and test. The simulated and measured axial ratios of the DRA in the direction of +z-axis ( ) are demonstrated in Fig. 17. As can be observed from the figure, the measured 3 dB axial ratio bandwidth for LHCP mode and RHCP mode are 30.4% (2.23-3.03 GHz) and 32.9% (2.17-3.02 GHz), respectively, while the simulated AR bandwidth for both CP states is 33.9% (2.18-3.07 GHz).

The simulated and measured radiation patterns of the proposed cylindrical DRA at two agile CP modes of 2.45 GHz are shown in Fig.18. As indicated in both figures, the antenna

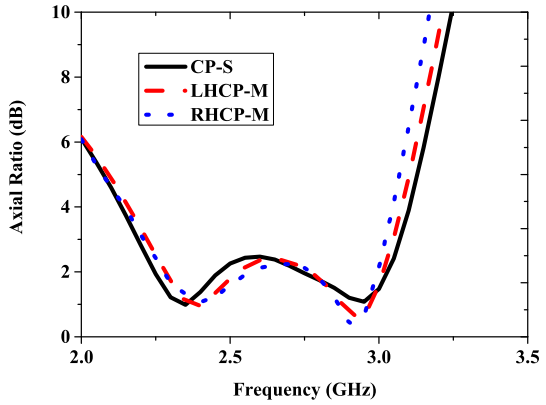

FIGURE 17. Simulated and measured axial ratios when the proposed DRA is configured at CP states.

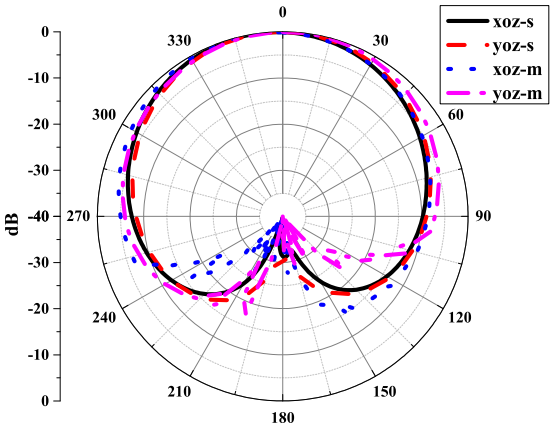

(a)

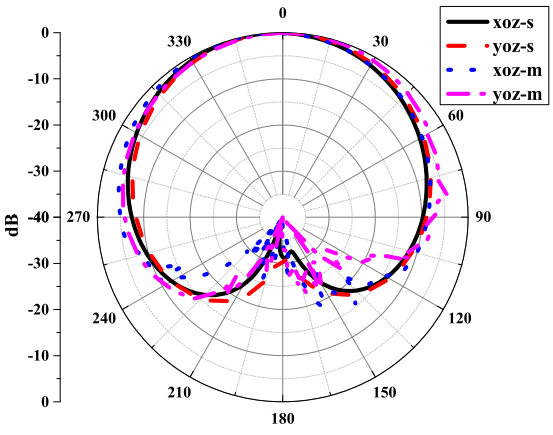

(b)

FIGURE 18. Simulated and measured normalized radiation patterns when the proposed DRA is configured at CP states of 2.45 GHz: (a) LHCP state and (b) RHCP state.

has broadside radiation patterns with maximum direction near +z-axis in both xoz-plane and yoz-plane, as expected. Moreover, the good consistency between simulations and measurements is observed in the main radiation direction ($\phi = 0°, \theta = 0°$) and some differences occur around the radiated zero-point, which are mainly susceptible to the non-uniform distributed dc wires between the proposed DRA and dc power. Radiation patterns at other frequencies were also simulated and measured, and very stable directional performance was found across the passband.

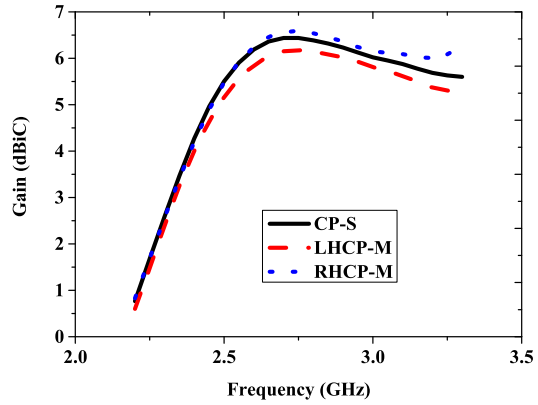

FIGURE 19. Simulated and measured gains when the proposed DRA is configured at CP states.

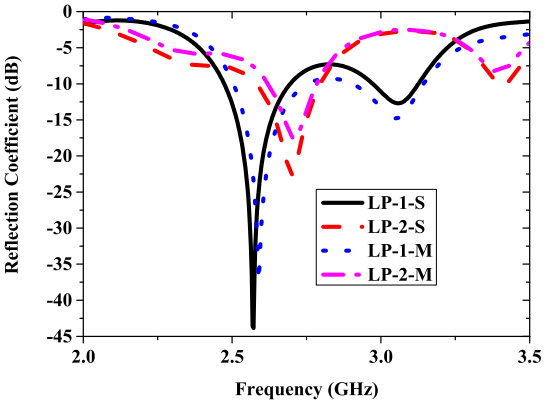

FIGURE 20. Simulated and measured input reflection coefficients when the proposed DRA is configured at LP states.

Fig. 19 plots the simulated and measured antenna gains, and reasonable consistency between them is concluded. The measured peak gains for LHCP state and RHCP state are 6.18 dBiC and 6.58 dBiC both at 2.75 GHz, well in accordance with the simulated counterpart of 6.44 dBiC at 2.7 GHz. The uncertainty in the gain measurement attributes to the slight test error of transmission coefficient in the microwave anechoic chamber and the inaccurate gain curve of standard horn published by manufacturer.

B. LINEAR-POLARIZED STATES

Fig. 20 depicts the simulated and measured input reflection coefficients when the proposed antenna is configured at LP states. The impedance bandwidths at two LP states are 9.5% (2.50-2.75 GHz) and 6.3% (2.62-2.79 GHz), which show good consistencies with simulations of 8.5% (2.47-2.69 GHz) and 8.2% (2.58-2.80 GHz), respectively. The far-field radiation patterns of the proposed polarization-reconfigurable DRA operated at LP states of corresponding resonant frequencies in both the xoz- and yoz- elevation planes are

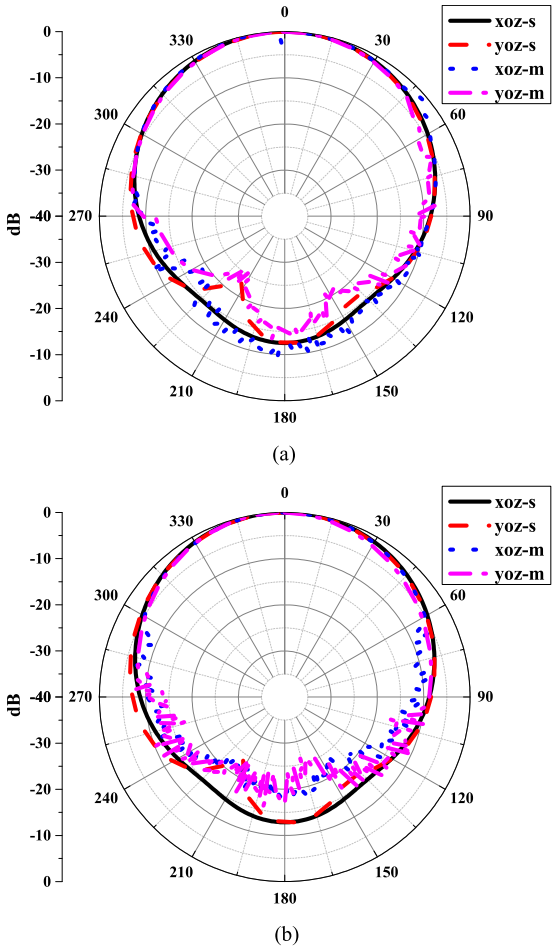

FIGURE 21. Simulated and measured normalized far-field radiation patterns when the proposed DRA is configured at LP states: (a) LP-1 state (active short shifters) of 2.55 GHz and (2) LP-2 state (active long shifters) of 2.7 GHz.

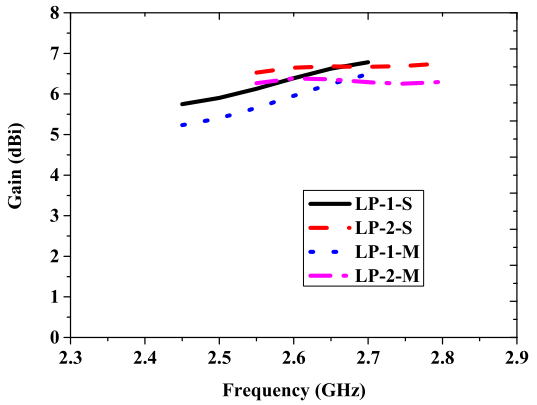

FIGURE 22. Simulated and measured gains when the proposed DRA is configured at LP states.

depicted in Fig. 21. Similar broadside pattern characteristics with main lobe direction to CP states are observed, but each pattern of LP states has litter side lobe with front to back ratio around 17.7 dB.

Fig. 22 shows the simulated and measured gains within the operation bandwidths of two LP states, and the maximum gains are 6.48 dBi and 6.39 dBi, respectively. Reasonable agreement between simulations and measurements is observed, and the slight differences can be attributed to the same reasons that lead to the performance discrepancy of CP states discussed in Section III A. From the above, the proposed DRA configured at LP states demonstrates frequency reconfigurable performance with two different bandwidth states under similar radiation patterns, which contributes to design compound reconfigurable DRA with multiple parasitic elements.

TABLE 2. Performance comparison with other polarization-reconfigurable DRAs.

Ref.	Polarization State	-10 dB BW	3 dB AR BW	Mech.	Gain
[29]	LHCP	22%	1%	PIN	4 dBiC
	RHCP	28%	1%		4 dBiC
	LP-1	21%	-		5 dBi
	LP-2	27%	-		5 dBi
[30]	LHCP	28.4%	21.1%	PIN	7.35 dBiC
	RHCP	27.6%	20.7%		7.35 dBiC
	LP	30.1%	-		7.44 dB
[31]	LHCP	35.6%	16.3%	Liquid	5 dBiC
	RHCP	35.6%	16.3%		5.5 dBiC
Our work	LHCP	34.3%	30.4%	PIN	6.18 dBiC
	RHCP	36.6%	32.9%		6.58 dBiC
	LP-1	9.5%	-		6.48 dB
	LP-2	6.3%	-		6.39 dB

BW: Bandwidth, AR: Axial Ratio, Mech.: Mechanism

C. PERFORMANCE ANALYSIS

Performance comparisons between the proposed DRA and previously published polarization-reconfigurable DRAs are listed in Table 2. It can be found that the proposed antenna exhibits better CP operating bandwidth, especially for axial ratio bandwidth, than those DRAs of [29] and [30]. Although the impedance bandwidth of [31] with liquid mechanism is slight wider than the proposed DRA, the axial ratio is significantly less than the one in this paper and the proposed DRA can not only achieve CP but also achieve LP with the realized gain above 6 dB for all states. In addition, the proposed DRA has a compact size of $0.55\lambda \times 0.55\lambda \times 0.14\lambda$. As mentioned in the introduction, the proposed cylindrical DRA with polarization reconfigurable characteristic has flexible states, wideband axial ratio performance, low complexity, and ease to fabricated and control.

IV. CONCLUSION

In this paper, a design method of polarization reconfigurable DRA based on tunable feed network with Wilkinson equal power distributor and selectable phase shifters has been proposed, which features agile polarization characteristics among LHCP state, RHCP state and two LP states with different resonant frequencies. The cylindrical DR operated at $HEM_{11\delta}$ mode and the wideband tunable feed network contributes to the wideband CP performance. It is worth mentioning that the operating frequency is arbitrary designated, and the proposed design can be rescaled and applied

straightforwardly to other frequencies of interest. A prototype of the proposed polarization reconfigurable cylindrical DRA operated at WLAN band is designed, fabricated and tested. The test results of the impedance bandwidth, 3 dB axial ratio bandwidth, radiation pattern, and gain verifies the effectiveness of the proposed polarization agility performance for DRA, showing a good agreement with simulations. The proposed reconfigurable DRA design exhibits potential characteristics of wide CP bandwidth and frequency switching LP bandwidth, making it a promising candidate for smart communication system applications.

REFERENCES

[1] S. Long, M. McAllister, and L. Shen, "The resonant cylindrical dielectric cavity antenna," *IEEE Trans. Antennas Propag.*, vol. AP-31, no. 3, pp. 406–412, May 1983.
[2] R. K. Mongia and P. Bhartia, "Dielectric resonator antennas—A review and general design relations for resonant frequency and bandwidth," *Int. J. Micro. Millimeter-Wave Comput.-Aided Eng.*, vol. 4, no. 3, pp. 230–247, 1994.
[3] K. M. Luk and K. W. Leung, *Dielectric Resonator Antennas*. Baldock, U.K.: Research Studies Press, 2003.
[4] A. Petosa, *Dielectric Resonator Antenna Handbook*. Norwood, MA, USA: Artech House, 2007.
[5] A. Petosa and A. Ittipiboon, "Dielectric resonator antennas: A historical review and the current state of the art," *IEEE Antennas Propag. Mag.*, vol. 52, no. 5, pp. 91–116, Oct. 2010.
[6] L. F. Zou, D. Abbott, and C. Fumeaux, "Omnidirectional cylindrical dielectric resonator antenna with dual polarization," *IEEE Antennas Wireless Propag. Lett.*, vol. 11, pp. 515–518, 2012.
[7] Y. X. Sun and K. W. Leung, "Dual-band and wideband dual-polarized cylindrical dielectric resonator antennas," *IEEE Antennas Wireless Propag. Lett.*, vol. 12, pp. 384–387, 2013.
[8] M. Zou and J. Pan, "Wideband hybrid circularly polarised rectangular dielectric resonator antenna excited by modified cross-slot," *Electon. Lett.*, vol. 50, no. 16, pp. 1123–1125, 2014.
[9] B.-J. Liu, J.-H. Qiu, C.-L. Wang, and G.-Q. Li, "Pattern-reconfigurable cylindrical dielectric resonator antenna based on parasitic elements," *IEEE Access*, vol. 5, pp. 25584–25590, 2017.
[10] D. Hou, J. Chen, P. Yan, and W. Hong, "A 270 GHz×9 multiplier chain MMIC with on-chip dielectric-resonator antenna," *IEEE Trans. Antennas Propag.*, vol. 8, no. 2, pp. 224–230, Mar. 2018.
[11] J. T. Bernhard, *Reconfigurable Antennas*. London, U.K.: Morgan & Claypool, 2007.
[12] M.-C. Tang, Z. Wen, H. Wang, M. Li, and R. W. Ziolkowski, "Compact, frequency-reconfigurable filtenna with sharply defined wideband and continuously tunable narrowband states," *IEEE Trans. Antennas Propag.*, vol. 65, no. 10, pp. 5026–5034, Oct. 2017.
[13] M. A. Hossain, I. Bahceci, and B. A. Cetiner, "Parasitic layer-based radiation pattern reconfigurable antenna for 5G communication," *IEEE Trans. Antennas Propag.*, vol. 65, no. 12, pp. 6444–6452, Dec. 2017.
[14] S.-L. Chen, F. Wei, P.-Y. Qin, Y. J. Guo, and X. Chen, "A multi-linear polarization reconfigurable unidirectional patch antenna," *IEEE Trans. Antennas Propag.*, vol. 65, no. 8, pp. 4299–4304, Aug. 2017.
[15] L. Ge, Y. Li, J. Wang, and C.-Y.-D. Sim, "A low-profile reconfigurable cavity-backed slot antenna with frequency, polarization, and radiation pattern," *IEEE Trans. Antennas Propag.*, vol. 65, no. 5, pp. 2182–2189, May 2017.
[16] M. H. Amini and H. R. Hassani, "Compact polarisation reconfigurable printed monopole antenna at 2.4 GHz," *Electon. Lett.*, vol. 49, no. 17, pp. 1049–1050, 2013.
[17] S. W. Lee and Y. J. Sung, "Simple polarization-reconfigurable antenna with T-shaped feed," *IEEE Antennas Wireless Propag. Lett.*, vol. 15, pp. 114–117, 2016.
[18] S.-G. Zhou, G.-L. Huang, H.-Y. Liu, A.-S. Lin, and C.-Y.-D. Sim, "A CPW-fed square-ring slot antenna with reconfigurable polarization," *IEEE Access*, vol. 6, pp. 16474–16483, 2018.
[19] Y. Sung, "Polarisation diversity antenna with asymmetrical Y-shaped feed structure," *Electon. Lett.*, vol. 49, no. 24, pp. 1512–1513, 2013.
[20] M. N. Osman, M. K. A. Rahim, M. R. Hamid, M. F. M. Yusoff, and H. A. Majid, "Compact dual-port polarization-reconfigurable antenna with high isolations for MIMO application," *IEEE Antennas Wireless Propag. Lett.*, vol. 15, pp. 456–459, 2016.
[21] K. X. Wang and H. Wong, "A reconfigurable CP/LP antenna with cross-probe," *IEEE Antennas Wireless Propag. Lett.*, vol. 16, pp. 669–672, 2017.
[22] K. L. Chung, S. Xie, Y. Li, R. Liu, S. Ji, and C. Zhang, "A circular-polarization reconfigurable Meng-shaped patch antenna," *IEEE Access*, vol. 6, pp. 51419–51428, 2018.
[23] W. Lin and H. Wong, "Multipolarization-reconfigurable circular patch with L-shaped probes," *IEEE Antennas Wireless Propag. Lett.*, vol. 16, pp. 1549–1552, 2017.
[24] W. C. Yang, W. Q. Che, H. Y. Jin, W. J. Feng, and Q. Xue, "A polarization-reconfigurable rotation AMC structure," *IEEE Trans. Antennas Propag.*, vol. 63, no. 12, pp. 5215–5305, Dec. 2015.
[25] Y.-M. Cai, S. Gao, Y. Yin, W. Li, and Q. Luo, "Compact-size low-profile wideband circularly polarized omnidirectional patch antenna with reconfigurable polarizations," *IEEE Trans. Antenna Propag.*, vol. 64, no. 5, pp. 2016–2021, May 2016.
[26] W. Lin and H. Wong, "Wideband circular polarization reconfigurable antenna," *IEEE Trans. Antennas Propag.*, vol. 65, no. 12, pp. 5938–5944, Dec. 2015.
[27] F. Wu and K. M. Luk, "Single-port reconfigurable magneto-electric dipole antenna with quad-polarization diversity," *IEEE Trans. Antennas Propag.*, vol. 65, no. 5, pp. 2289–2296, May 2017.
[28] L. Ge, X. Yang, M. Li, and H. Wong, "Polarization-reconfigurable magnetoelectric dipole antenna for 5G Wi-Fi," *IEEE Antennas Wireless Propag. Lett.*, vol. 16, pp. 1504–1507, 2017.
[29] S. Dhar, K. Patra, R. Ghatak, B. Gupta, and D. R. Poddar, "Reconfigurable dielectric resonator antenna with multiple polarisation states," *IET Microw., Antennas Propag.*, vol. 12, no. 6, pp. 895–902, May 2018.
[30] W.-W. Yang, X.-Y. Dong, W.-J. Sun, and J.-X. Chen, "Polarization reconfigurable broadband dielectric resonator antenna with a lattice structure," *IEEE Access*, vol. 6, pp. 21212–21219, 2018.
[31] Z. Chen and H. Wong, "Liquid dielectric resonator antenna with circular polarization reconfigurability," *IEEE Trans. Antennas Propag.*, vol. 66, no. 1, pp. 444–449, Jan. 2018.

BEI-JIA LIU was born in Heilongjiang, China, in 1988. She received the B.S. degree in communication engineering from the Harbin University of Science and Technology, Harbin, China, in 2010, and the M.S. degree in information and communication engineering from the Harbin Institute of Technology, Harbin, in 2013, where she is currently pursuing the Ph.D. degree in electromagnetic field and microwave technology.

She joined the Harbin Institute of Technology, as an Assistant Engineer, in 2013, and was promoted to an Engineer, in 2016. Her research interests include dielectric resonator antenna and reconfigurable antenna.

JING-HUI QIU was born in Heilongjiang, China, in 1960. He received the B.S. degree in radio engineering, and the M.S. and Ph.D. degrees in communication and information systems from the Harbin Institute of Technology, in 1982, 1987, and 2008.

From 1982 to 1987, he was a Teaching Assistant with the Harbin Institute of Technology. From 1987 to 1992, he was promoted as a Lecturer, and then, became an Associate Professor. He was promoted as a Professor, in 2002. He has authored or coauthored over 100 publications, including book chapters, journal papers, and conference articles. His research interests include electromagnetic theory, microwave devices, antennas, and millimeter-wave imaging.

CHANG-HUI WANG was born in Inner Mongolia, China, in 1996. She received the B.S. degree in electromagnetic field and wireless technology from the Harbin Institute of Technology, Harbin, China, in 2018. She is currently pursuing the M.S. degree in electromagnetic field and microwave technology. Her research interests include dielectric resonator antenna and metasurface.

WEI LI was born Heilongjiang, China, in 1979. He received the B.S. degree in communication engineering, the M.S. degree in electromagnetic field and microwave technology, and the Ph.D. degree in information and communication engineering from the Harbin Institute of Technology, in 2002, 2005, and 2010, respectively.

He has been a Lecturer with the School of Electronics and Information Engineering, Harbin Institute of Technology, since 2010. His research interests include antenna miniaturization technology and ultra-wideband antenna.

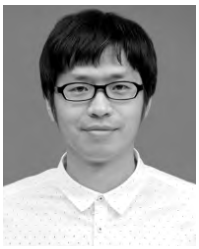

GUO-QIANG LI was born in Heilongjiang, China, in 1985. He received the B.S. degree in information and computing science from Northeast Agriculture University, Harbin, China, in 2008, and the M.S. degree in applied mathematics from Harbin Engineering University, Harbin, in 2011.

From 2011 to 2014, he was with Zhongxing Telecommunication Equipment Corporation. He has been with Harbin Kejia General Mechanical and Electrical Company, Harbin, as an Engineer, since 2014. His research interests include information fusion image recognition algorithm, millimeter-wave imaging, and electromagnetic field theory.